Selective adsorption behavior of Cd^{2+} imprinted acrylamide-crosslinked-poly(alginic acid) magnetic polymers: fabrication, characterization, adsorption performance and mechanism

Zuyu Li, Shuangzhen Guo, Da Li and Lihua Zang

ABSTRACT

Poly(acrylamide) grafted and glutaraldehyde-crosslinked alginic acid nano-magnetic adsorbent (AAMA) was prepared by selecting Cd^{2+} as a template ion. Scanning electron microscope (SEM), thermo-gravimetric analyzer (TGA), vibrating sample magnetometer (VSM) and infrared spectroscopy (IR) were used to characterize the morphology and structure of AAMA. The adsorption of AAMA for different metal ions was compared and the impact of various factors for adsorption of Cd^{2+} was systematically investigated. These results suggested that the AAMA was the aggregates of Fe_3O_4 nanoparticles with a diameter of about 50–100 nm and had selectivity for Cd^{2+} adsorption. The maximum adsorption capacity for Cd^{2+} is 175 mg/g at pH 5.0 and 303 K. The experimental data were well described by the Langmuir isotherm model and pseudo-second-order model. The parameters of adsorption thermodynamics concluded that the adsorption progress is spontaneous and endothermic in nature. The parameters of adsorption activation energy suggested that there is physical adsorption and chemisorption on the adsorption of metal ions. AAMA could be regenerated by EDTA and still keep 71% adsorption capacity in the fifth consecutive adsorption-regeneration cycle. Therefore, AAMA would be useful as a selective and high adsorption capacity nano-magnetic adsorbent in the removal of Cd^{2+} from wastewater.

Key words | alginic acid, Cd^{2+} template ion, magnetic adsorbent, select adsorption

Zuyu Li
Shuangzhen Guo (corresponding author)
Da Li
Lihua Zang
College of Environmental Science and Engineering,
Qilu University of Technology (Shandong Academy
of Sciences),
Jinan, 250353,
China
E-mail: guosz@qlu.edu.cn

HIGHLIGHTS

- A novel poly(acrylamide) grafted and glutaraldehyde-crosslinked alginic acid nano magnetic adsorbent was prepared and used for selective adsorption of Cd^{2+}.
- The maximum adsorption capacity for Cd^{2+} is 175 mg/g, which was more 4.79 times that for any other heavy metal ions.
- AAMA selectively adsorbs Cd^{2+}, which not only relies on the ion cavity, but also depends on functional groups.

INTRODUCTION

Heavy metal ions in water have been a major preoccupation for many years because of toxicity to biology and the eco-system threat. Cadmium cannot be degraded by microorganisms and can be accumulated in biology. It is considered as one of the most toxic metals. Cadmium is carcinogenic, it can cause dyspnea, lung fibrosis, testicular degeneration and chronic lung disease (Ahmaruzzaman 2011). Therefore, cadmium removal from wastewater has become a greatly significant subject today. Researchers have developed many technologies and methods for cadmium removal from wastewater including chemical precipitation, reverse osmosis, membrane separation,

adsorption, and electrodialysis (Uddin 2017). Considering the efficiency and economy points of view, adsorption is one of the most widely used and promising methods for cadmium removal.

Alginic acid is extracted from brown algae, one of the most abundant natural polymers. Alginic acid has three different functional groups, including hydroxyl, ether and carboxyl. The type, source, and vegetation conditions of alginic acid have an impact on the arrangements of mer units. There are more than 200 kinds of alginate in the market. Alginic acid has been widely used in the food, pharmaceutical, and cosmetic industry due to its stabilizing properties and gelling abilities. Alginic acid, with its good coordination ability, can be applied to remove cadmium ions from effluent (Vaid *et al.* 2015). It is well known that alginic acid can form a three-dimensional coordination bond with cadmium ions. Moreover, the adsorption capacity of brown algae biomass biosorbent and its chemical modifiers have been investigated by many researchers. Matheickal *et al.* revealed the adsorptive property of heavy metal ion biosorbents using *Ecklonia radiata* and *Durvillaea potatorum*. In addition to metal ion chelation, alginic acid has advantageous physicochemical properties that affect its high attention in polymer research (Pawar & Edgar 2012). However, unsatisfying mechanical properties and water dispersion have limited its applications as an adsorbent (Mahesh *et al.* 2011). In order to solve the question of water dispersion, alginic acid is often chemically modified by crosslinking with suitable cross linkers or introducing amide. Nevertheless, the adsorption capacity of crosslinked alginic acid for heavy metal ions would decrease because of the hydroxyl and hydroxy groups that are located on alginic acid (Ge & Huang 2010). Therefore, in order to increase the adsorption capacity of the crosslinked alginic acid, it must be grafted with more functional groups such as thiol, carboxyl and amine (Yong *et al.* 2013).

Ion imprinting technology is the development of the adsorption method. The ion imprinting technique is used to prepare crosslinked metal complexed polymers, in which a regulator for cross-linking and the metal cation acts as a template. Ion-imprinted polymer has selectivity performance and great adsorption capacity for target metal ions. Recently, precipitation polymerization, bulk polymerization, surface imprinting, emulsion polymerization and suspension polymerization have been applied to prepare ion-imprinted polymer (Lenoble *et al.* 2015). Different metal ions have been used as template ions. Various metal ion-imprinted polymers have been used to adsorb specific metal ions, compared with a control group lacking metal

ions in preparation of adsorbent, the adsorption capacity of imprinted polymers showing to be significantly enhanced. Various polymers have acted as imprinted polymers, such as chitosan, acrylamide (Zhu *et al.* 2017), mesoporous silica and carbon nanofiber (Mishra & Verma 2017). To our knowledge, there are no researchers that have selected alginic acid as an imprinted polymer.

Herein, acrylamide grafted and glutaraldehyde-cross-linked alginic acid nano magnetic adsorbent (AAMA) was prepared by selecting Cd^{2+} as a template ion. FT-IR, TGA, SEM, TEM, VSM and XRD were applied to characterize the properties of AAMA. The adsorption capacity of AAMA for Cd^{2+} was tested by batch experiments. Various factors such as pH, kinetics, isotherms and reuse of AAMA were investigated.

MATERIALS AND METHOD

Materials

Alginic acid, acrylic amide (AA), ammonium persulfate and potassium persulfate (KPS) were obtained from China Xiya Reagent Corporation Ltd (Shang-hai, China). The metal salts $(Pb(NO_3)_2$, $Cd(NO_3)_2$, $Cu(NO_3)_2$, $Co(NO_3)_2$, $Zn(NO_3)_2$ and $HgCl_2$ were obtained from Guoyao Chemical Reagents Corporation Ltd (Shang-hai, China). In this study, all other reagents were analytical grade and the water was deionized water.

Preparation of AAMA

Magnetic Fe_3O_4 was synthesized by the hydrothermal method (Guo *et al.* 2017).

1 g Fe_3O_4 was added in 210 mL distilled water with ultrasound for 15 min. Then, 3 g alginic acid and 1.5 g NaOH were added in solution. After adding 25 mL glutaraldehyde, the mixture was reacted with stirring for 2 h at 40 °C. 6.2 g acrylic amide was added into the mixed solution for 30 min under stirring. By adding 3 mol/L hydrochloric acid, the pH of the solution was adjusted to 5. After adding 0.4 g $Cd(NO_3)_2$, the mixture was heated to 60 °C with stirring for 0.5 h under a nitrogen stream. Afterwards, 0.2 g ammonium persulfate and 0.2 g KPS were mixed into the solution. The mixture was warmed to 80 °C and kept stirring for 4 h. After the reaction, the suspension was separated by the use of a magnet. The solid was washed several times with distilled water, acetone and ethanol in sequence, and dried at 65 °C for 12 h under vacuum. The obtained brown product contained the template Cd^{2+} and was named Cd-AAMA. After

being ground, the product was immersed in 0.5 mol/L EDTA solution to remove the template Cd^{2+} ion. The magnetic brown solid was separated by use of a magnet and washed with distilled water, then dried at 65 °C in a vacuum. The obtained brown product was named AAMA. The possible preparation processes are given in Figure 1.
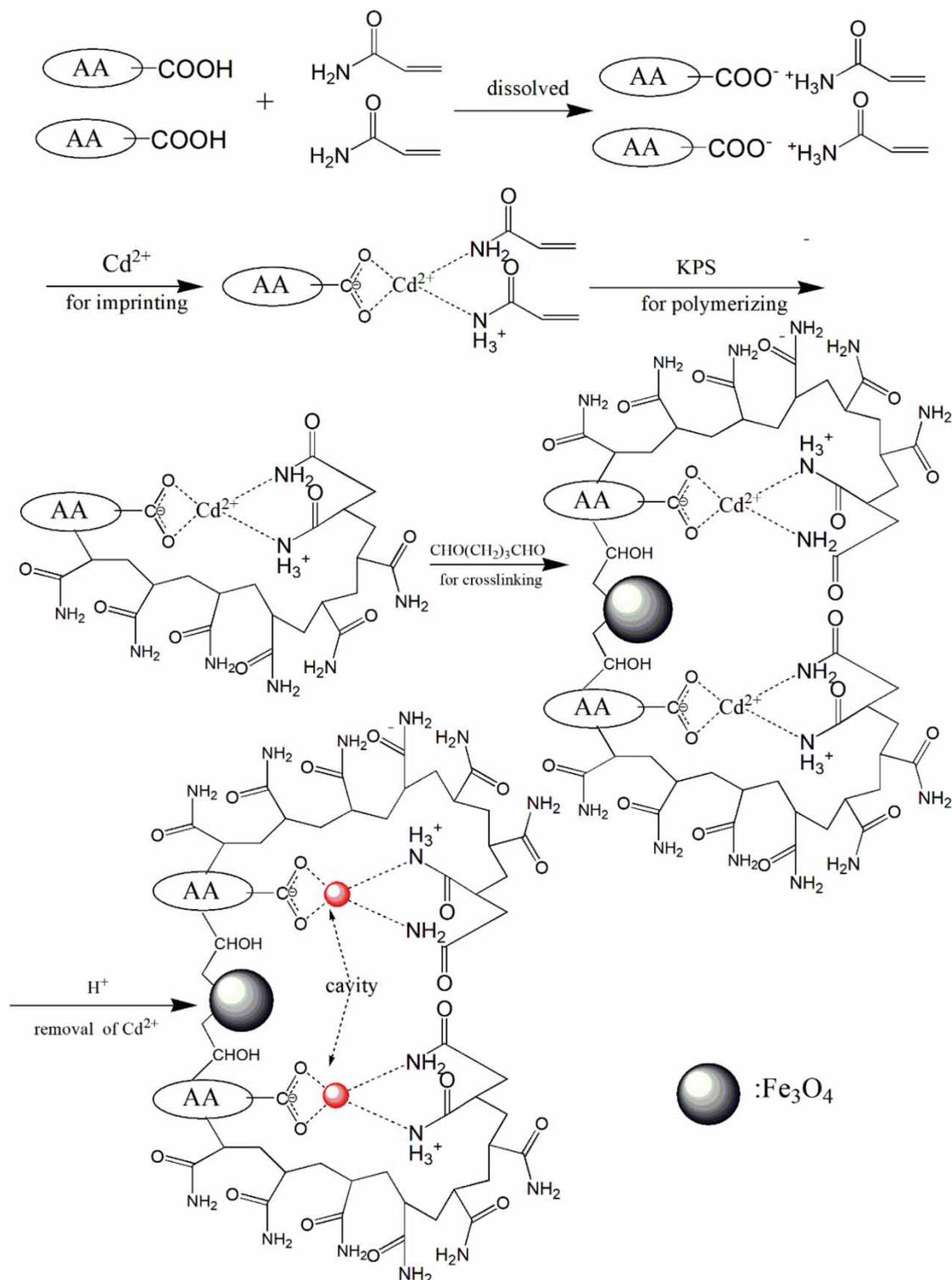

Figure 1 │ The synthetic route of AAMA.

Characterization of AAMA

The hysteresis loops were detected by vibrating sample magnetometer (VSM) (LDJ 9600, USA). Fourier transform infrared (FTIR) spectrograms were obtained by Perkin Elmer spectrum FTIR (Perkin Elmer, USA). SEM images were photographed by Sigma (Carl Zeiss, Germany). The thermal stability of AAMA was tested by thermogravimetric analysis (TGA) (SDTA851, Swit). The concentration of metal ions was detected by Inductively coupled plasma mass spectrometry (ICP-MS) (Agilent 7500, USA).

Adsorption experiments

Aqueous solutions of metal ions (concentration:100 mg/L) were prepared from Pb(NO$_3$)$_2$, Cd(NO$_3$)$_2$, Cu(NO$_3$)$_2$, Co(NO$_3$)$_2$, Zn(NO$_3$)$_2$ and HgCl$_2$. 0.1 mol/L HCl and 0.1 mol/L NaOH were used to adjust the pH values of solution. Generally, 100 mg AAMA was added to 100 mL metal ion solutions and the mixture was subjected to ultrasound for 10 min and shocked for a certain time. The adsorption capacity q(mg/g) of AAMA was calculated as follows:

$$q = \frac{(c_0 - c_e) \cdot V}{m} \tag{1}$$

where C_e and C_0 (mg/L) are the equilibrium and initial concentration of metal ions, m (g) is the mass of AAMA, V (L) is the volume of aqueous solution. The isothermal and kinetic models used in the study are shown in Table 1.

Measurement of point of zero charge (PZC)

The PZC of AAMA was tested by the salt addition method. First, AAMA (100 mg) was added in 0.01 M NaNO$_3$ solution (100 mL). Second, NaOH (0.1 M) and HNO$_3$ (0.1 M) were used to adjust the pH of the suspension. Third, the mixed solution was continuously stirred for 24 h. Finally, the pH values were detected and the changes of the pH (ΔpH) plotted against the initial pH. The point where the plot bisects the x-ax is was the PZC of AAMA (Mahmood *et al.* 2011).

Desorption and regeneration studies

The adsorption experimental conditions: Cd^{2+} is 200 mg/L, contact time is 180 min, 100 mg AAMA in 100 mL solution at 303 K. After magnetic separation, AAMA that had adsorbed Cd^{2+} was added in 50 mL of 0. 5 mol L^{-1}EDTA and stirred for 6 h at 298 K. Afterwards, the AAMA was magnetically separated from the solution and washed several times with distilled water. AAMA was reused in a new adsorption-desorption cycle and recycled five times.

RESULTS AND DISCUSSIONS

Characterization of AAMA

Figure 2 shows the SEM image of Fe$_3$O$_4$ and AAMA. Fe$_3$O$_4$ shows polyhedral morphology. AAMA has an irregular

Table 1 │ The kinetic and isothermal adsorption models used in the study

Model	Linear equation	Plot	Nomenclature	Reference
Kinetic model				
Pseudo first-order	$\log(q_e - q_t) = \log q_e - \dfrac{K_1 t}{2.303}$	$\log(q_e - q_t)$ vs. t	q_e and q_t are the amounts of adsorbed by adsorbent at equilibrium and time t, respectively; K_1 is the pseudo first-order rate constant.	Ge *et al.* (2016)
Pseudo second-order	$\dfrac{t}{q_t} = \dfrac{1}{K_2(q_e)^2} + \dfrac{t}{q_e}$	t/q_t vs. t	K_2 is the pseudo second-order rate constant	Ge & Huang (2010)
Intraparticle diffusion	$q_t = K_i t^{0.5} + C$	q_t vs $t^{0.5}$	C is a constant.	Guo *et al.* (2017)
Isotherm model				
Freundlich	$\log q_e = \log K_F + \dfrac{\log C_e}{n}$	$\log q_e$ vs. $\log C_e$	K_F is a Freundlich constant; n is a constant depicting the adsorption intensity	He *et al.* (2016)
Langmuir	$\dfrac{C_e}{q_e} = \dfrac{1}{q_m \cdot K_L} + \dfrac{C_e}{q_m}$	C_e/q_e vs. C_e	K_L is the adsorption equilibrium constant	Guo *et al.* (2020)
Dubinin-Raduskevich	$\ln q_e = \ln q_m - BA^2$	$\ln q_e$ vs. A	B is a Dubinin-Raduskevich model constant	Pang *et al.* (2011a)
Redlich-Petterson	$q_e = \dfrac{K_{RP} C_e}{1 + a_p C_e^{\beta}}$	q_e vs C_e	K_{RP}, a_p and β are Redlich-Petterson model constants and the exponent.	Zhu *et al.* (2017)

block morphology with pores inside and granular protrusions on the surface. Figure 2(c)–2(e) show the higher magnification TEM images of AAMA; it clear to observe

that Fe$_3$O$_4$ is distributed in AAMA. Moreover, the observed lattice fringes indicate that Fe$_3$O$_4$ has a good crystalline structure (Figure 2(e)). The fringe spacing of 0.25 nm could
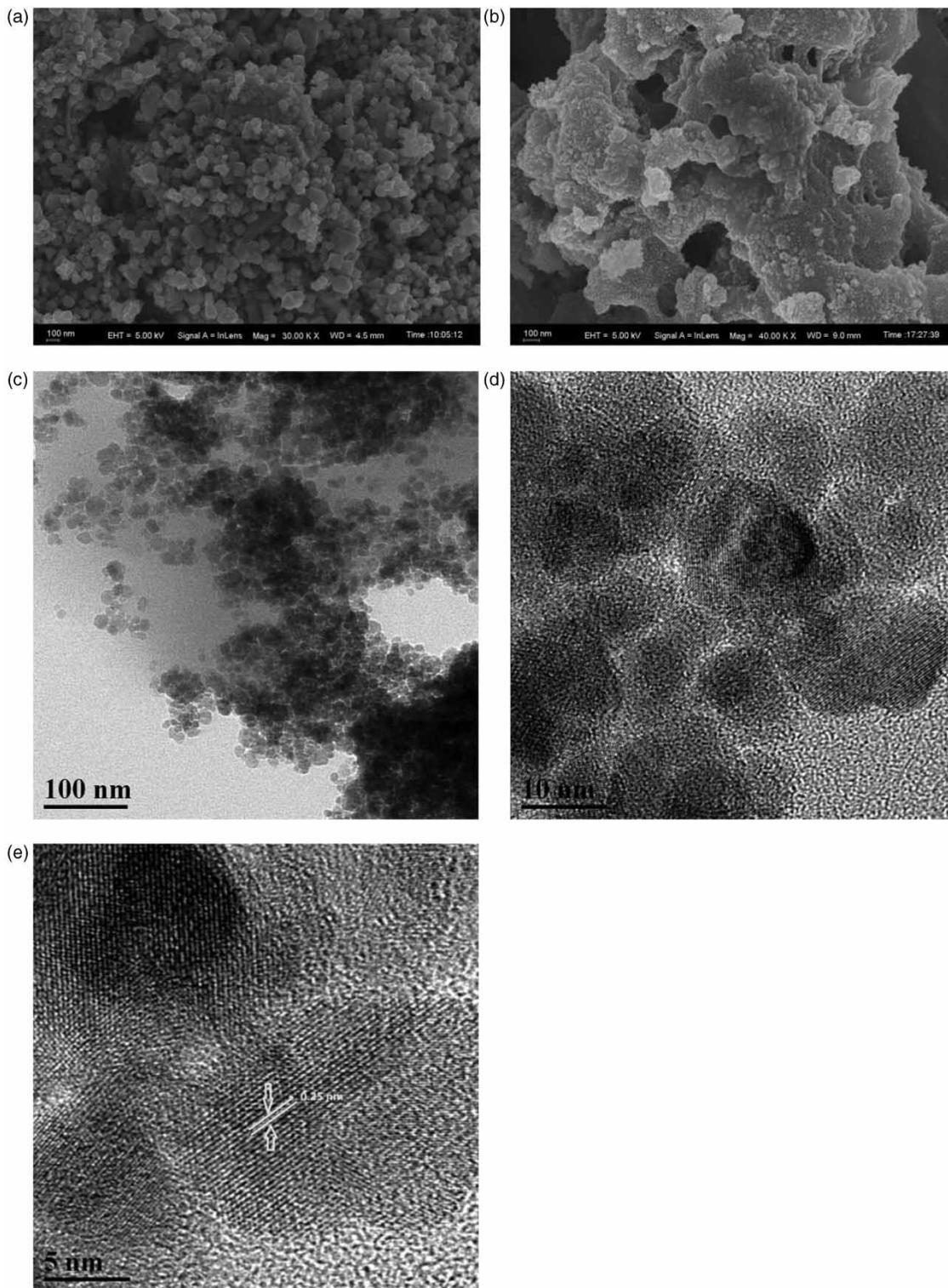

Figure 2 | SEM image of Fe$_3$O$_4$ (a) and AAMA (b), TEM image of AAMA (c-e).

be corresponded to the (311) plane of Fe$_3$O$_4$ (Guo *et al.* 2020). This clearly testified that Fe$_3$O$_4$ has combined with AAMA. The EDX results of AAMA are shown in Figure S1 and Table S1. It clear to observe that AAMA is rich in N, O elements, which is advantageous for the adsorption of metal ions. The Fe and O elements are also shown in Figure S1, suggesting Fe$_3$O$_4$ has combined with alginic acid.

Figure 3 shows the XRD results of Fe$_3$O$_4$ and AAMA. The peaks of Fe$_3$O$_4$ are at 30.1 (220), 35.5 (311), 43.1 (400), 53.4 (422), 57.0 (511) and 62.6 (440), which agreed with the data of Fe$_3$O$_4$ in the JCPDS file (PDF No. 85-1436). This proved that Fe$_3$O$_4$ has a spinel structure. The characteristic peaks of AAMA are identified with Fe$_3$O$_4$ except the peaks at 27.2, indicating that the grafted alginic acid does not influence the crystal structure of Fe$_3$O$_4$. Moreover, the XRD results of AAMA confirmed each other with SEM diffraction fringes.

To confirm the functional group in AAMA, the FTIR spectra of prepared intermediate and AAMA are shown in Figure 4. The FTIR spectra of Fe$_3$O$_4$, Fe$_3$O$_4$ + AA, Fe$_3$O$_4$ + AA + AM, Fe$_3$O$_4$ + AA + AM + Cd^{2+} and AAMA revealed a pointed absorbance band at 576 cm^{-1}, corresponding to the stretching vibration of Fe-O. The peak at 1,024 cm^{-1} corresponds to C-O stretching vibration, indicating a crosslinking reaction between epoxy chloropropane and functional monomers (Zhu *et al.* 2017). The absorbance peaks of AA, Fe$_3$O$_4$ + AA, Fe$_3$O$_4$ + AA + AM, Fe$_3$O$_4$ + AA + AM + Cd^{2+} and AAMA at 1,640 cm^{-1}, 1,409 cm^{-1} and 2,941 cm^{-1} were attributed to the stretching of C=O of acrylamide, bending vibration and stretching vibration of C-H. Peaks at 3,649 cm^{-1} and 1,155 cm^{-1} are contributing to N-H stretching vibration and the weak swing vibration of NH$_2$, respectively (Ge *et al.* 2016). In addition,
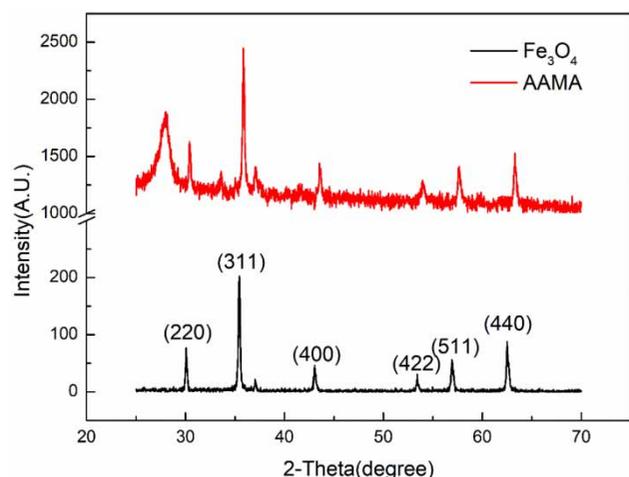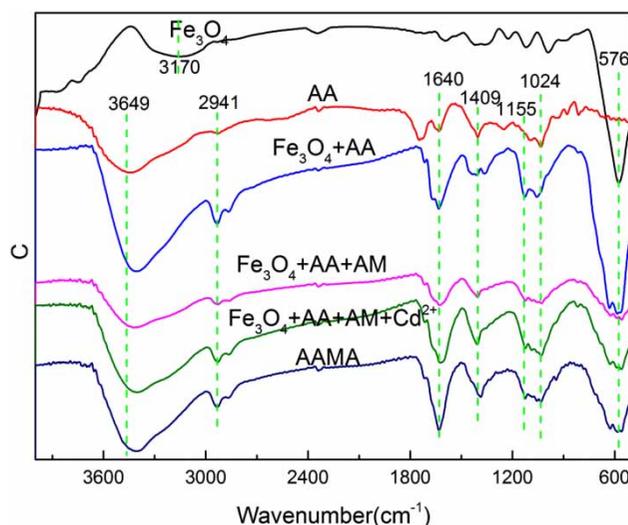

Figure 4 | The IR spectra of Fe$_3$O$_4$, AA, Fe$_3$O$_4$ + AA, Fe$_3$O$_4$ + AA + AM, Fe$_3$O$_4$ + AA + AM + Cd^{2+} and AAMA.

as the degree of crosslinking increases, the possibility of a six- or five-membered ring increases, resulting in a red-shift of the stretching vibration peak of the amino group. FTIR proved that the AAMA have successfully grafted acrylamide and alginic acid.

Figure 5 shows the TGA curves of prepared intermediate and AAMA. At 50 °C to 125 °C, the Fe$_3$O$_4$ had a weight loss of about 3.57%, corresponding to adsorbed water volatilization (Guo *et al.* 2017). In addition, the Fe$_3$O$_4$ had a weight loss of about 3.86% at range of 570 °C to 750 °C, which corresponds to hydroxyl decomposition. Compared to Fe$_3$O$_4$, Fe$_3$O$_4$ + AA reveals an additional thermal decomposition of 28.7% related to the decomposition of the amino group and carboxyl, which are located at AA (Pandi & Viswanathan 2015). Compared to Fe$_3$O$_4$ + AA, Fe$_3$O$_4$ + AA + AM shows an additional loss of
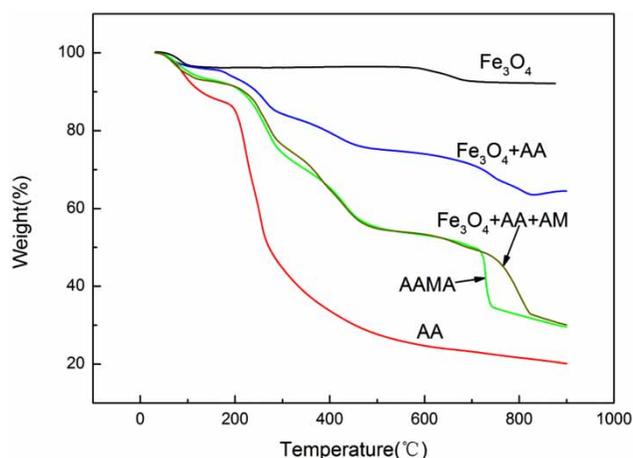

Figure 3 | XRD results of Fe$_3$O$_4$ and AAMA.

Figure 5 | TGA results of Fe$_3$O$_4$, AA, Fe$_3$O$_4$ + AA, Fe$_3$O$_4$ + AA + AM and AAMA.

30.2%, corresponding to the decomposition of AM. Fe_3O_4 + AA + AM and AAMA show higher consistency in thermal weight loss, except for the temperature range of 719–822 °C. This may be due to the fact that there are large amounts of ionic holes in AAMA, which increases the specific surface area and leads to rapid decomposition of the functional groups. Referring to the thermal decomposition of AA, it can be concluded that AAMA have been successfully prepared.

To test the magnetic characteristics of the AAMA, the magnetic saturation value of Fe_3O_4 and AAMA are tested at 298 K (Figure 6). The magnetization saturation values of the Fe_3O_4 and AAMA are 57.55 and 12.26 emu/g, respectively. According to the IR and TGA results, AA and AM are modified on the surface of Fe_3O_4. Since AA and AM are not magnetic, this will mask the magnetic properties of Fe_3O_4 (Ma *et al.* 2005). VSM results showed that the AA and AM had been grafted on the surface of Fe_3O_4.

Adsorption of AAMA for heavy metal ions

Table 2 shows the adsorption capacities of AAMA at pH 5 for different metal ions (Pb^{2+}, Hg^{2+}, Cu^{2+}, Cd^{2+}, Co^{2+} and Zn^{2+}). The adsorption capacity of AAMA for Cd^{2+} was more than 4.79 times that for any other heavy metal ions, which is higher than an other adsorbent (Ge *et al.* 2016). The results indicate th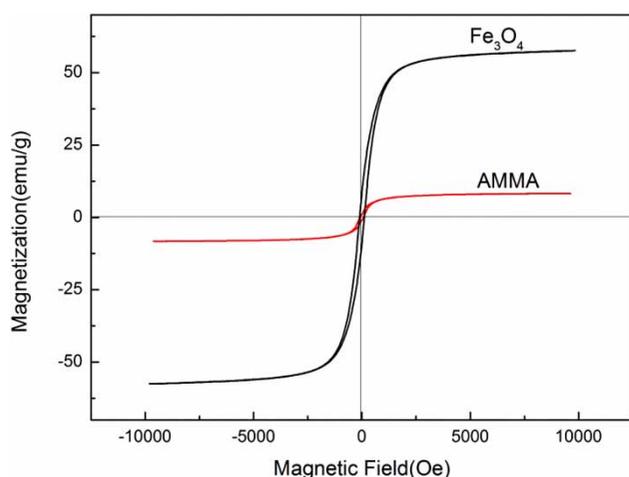at AAMA had selective adsorption toward Cd^{2+}. This selectivity is the reason for the reserve of holes and coordination (Figure 1).

Effect of factors for adsorption of Cd^{2+} by AAMA

Effect of pH

It is well recognized that the pH value of a solution plays an important part in the adsorption process. Figure 7 shows the change of the adsorption capacity of AAMA by varying the pH from 1.0 to 5.5. It can be discovered that the pH value of the solution has an intense effect on the adsorption capacity of AAMA. The adsorption capacity of AAMA for Cd^{2+} first increases rapidly at pH 1–5 and then decreases at pH 5–5.5. The maximum adsorption capacity of AMAA for Cd^{2+} at pH 5.0 achieved 165 mg/g. The other reports also showed this phenomenon (Ge *et al.* 2012). The adsorption capacity of AAMA is much higher than that of the composite material for Cd^{2+}, which reaches a maximum of 100.9 mg/g at pH 5.5 (Fan *et al.* 2020).

The influence of pH on the adsorption process is mainly impacted in the interaction between metal ions and functional groups. Point of zero charge (PZC) can reflect the surface charge characteristics of AAMA. When the pH value of the solution is lower than PZC, the surface charge of the adsorbent is positive, resulting in the access of metal ions becoming difficult due to repulsive forces. Because the PZC of AAMA was 4.7 (which is consistent with the zeta potential results, see Supporting information Figure S2), the surface charge of AAMA was positively charged; there was
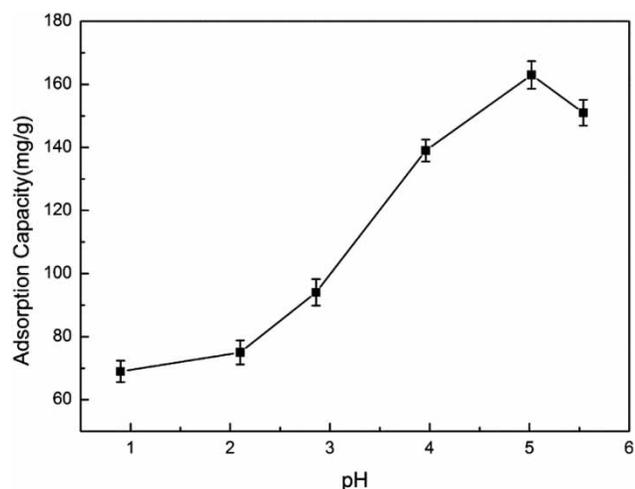
Figure 6 │ Magnetization curve of the magnetic Fe_3O_4 and AAMA measured at room temperature.

Table 2 │ The adsorption capacities of AAMA for different heavy metal ions

Metal ion	Cd^{2+}	Zn^{2+}	Co^{2+}	Cu^{2+}	Hg^{2+}	Pb^{2+}
Adsorption capacity (mg/g)	163	34	18	22	31	24

Figure 7 │ Effect of initial pH value on the adsorption capacity adsorption (experimental conditions: metal ion concentration is 200 mg/L, contact time is 140 min, 100 mg AAMA in 100 mL solution at 303 K, Repeat time: 3).

competition between metal ions and hydrogen ions on the AAMA when the pH values were below 4.7, leading to the lower adsorption capacity at solution pH below 4.7. When the pH values of the solution were higher than 4.7 the surface charge of AAMA was negative and Cd^{2+} was positively charged, so the adsorption capacity of AAMA increased thanks to the electrostatic attractive force between metal ions and functional groups (Lee *et al.* 2012). Moreover, the pH value of the solution would affect the chelation strength between functional groups and metal ions. With the increase of pH, Cd^{2+} began to precipitate as hydroxides. Therefore, 5.0 was selected as the optimum pH value for Cd^{2+} adsorption. In other studies, the adsorption capacity of Cd^{2+} was highest at pH 5.0 (Rahmi & Nurfatimah 2018).

Effect of AAMA dosage

Figure 8 shows the adsorption capacity of AAMA at different dosages. It can be found that the adsorption capacity of AAMA for Cd^{2+} slightly decreased with the increase in dosage (20–100 mg). Nevertheless, the adsorption capacity of AAMA quickly decreased in a dosage range of 100–140 mg. It might be the fact that AAMA could effectively contact with more Cd^{2+} in the same concentration of solution while the AAMA dosage was smaller. Mittal considered that the greater the amount added, the greater the probability of AAMA agglomeration, resulting in a decrease in the number of adsorption sites and a decrease in adsorption capacity (Mittal *et al.* 2015). In order to reduce the error caused by weighing as much as possible, the added amount is 100 mg in the experiment.
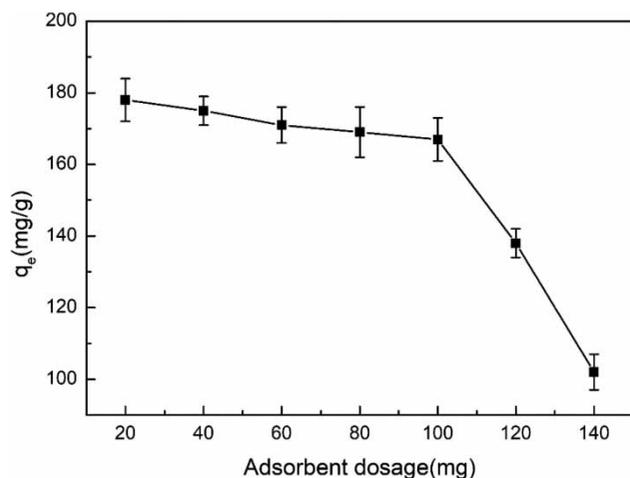
Effects of temperature and adsorption time on the adsorption capacity

The effect of temperature and adsorption time on the adsorption capacity for Cd^{2+} are shown in Figure 9. Obviously, a rapid initial rate of Cd^{2+} adsorption on the AAMA was discovered during the first 70 min, contributing to approximately 85% of the total adsorption capacity of AMAA, with a gradual approach to the limiting adsorption capacity at 140 min. In its infancy, the high initial adsorption rate contributed to strong chelation, the effective mass transfer and the abundant adsorption sites available (Jing *et al.* 2015). The spendable adsorption sites decreased with the increase in adsorption time and the travel rate slowed down gradually due to the reduction in concentration difference. Moreover, it can also be found that the adsorption capacity of AAMA was influenced by the temperature of the solution. With the increase in temperature, the adsorption capacity of AAMA for Cd^{2+} reflected the phenomenon of first increasing and then decreasing. When the temperature is 303 K, the adsorption capacity of AAMA for Cd^{2+} is largest. This may be due to the fact that the phenomenon of thermal expansion was discovered on AAMA when the temperature rises. In the temperature range of 298–303 K, with the increase in temperature, the metal ion diffusion rate increases, causing metal ions to enter the deeper part of the AAMA, and the ions' cavity utilization increases. Thereby the adsorption capacity is increased. However, in the temperature range of 303–308 K, AAMA undergoes thermal expansion. The ion cavities were squeezed with the expansion of AAMA, making
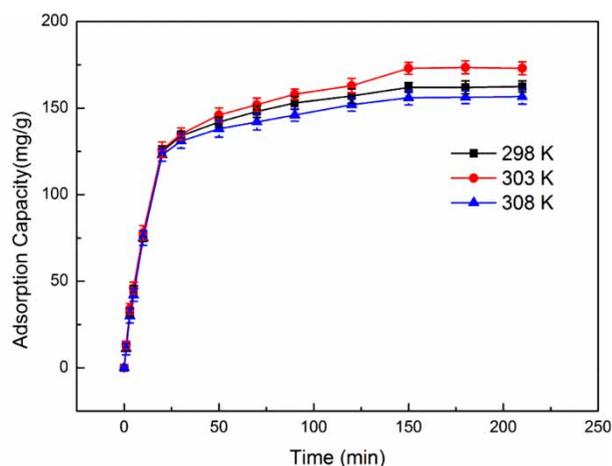
Figure 8 │ Effects of adsorbent dosage for the adsorption of Cd²⁺ on AAMA (experimental conditions: metal ion concentration is 200 mg/L(100 mL), pH = 5, contact time is 140 min, 303 K, repeat time: 3).

Figure 9 │ Effects of adsorption time and temperature on the adsorption capacity (experimental conditions: metal ion concentration is 200 mg/L, pH = 5, 100 mg AAMA in 100 mL solution, repeat time: 3).

it difficult for Cd^{2+} to enter them. Thereby, the adsorption capacity decreased. The adsorption of Pb^{2+} on crosslinked chitosan (Ge et al. 2016) and the adsorption of Cd^{2+} on β-cyclodextrin (Zhu et al. 2017) also found analogous results. Hence, AAMA had an optimal temperature (303 K) for the adsorption of Cd^{2+}.

Adsorption kinetics

In order to investigate the adsorption kinetics of the adsorption process, the pseudo-first-order kinetic model, pseudo-second-order kinetic model and intra-particle diffusion model were employed to fit the adsorption rate data.

The pseudo-first-order kinetic model and pseudo-second-order kinetic model are shown in Figure 10. Table 3 shows the results of correlation coefficients (R^2) and kinetic constants. From the point view of predicted q_e and fitting R^2, the pseudo-second-order model is more suitable than the pseudo-first-order model to describe the adsorption kinetics, indicating that the adsorption rate of Cd^{2+} is controlled by chemical progress (Pang et al. 2011a).

To further explore the adsorption mechanism, the intra-particle diffusion model is used to investigate the adsorption progress. Figure 11 shows the plots of q_t versus $t^{1/2}$ for Cd^{2+}. From Figure 11, the fitted linear can be divided into three stages. Table 4 shows the calculated intra-particle diffusion constants. From Table 4, it can be found that the order of

adsorption rate is $K_{id,1} > K_{id,2} > K_{id,3}$. The first stage is that Cd^{2+} is adsorbed in the ion cavities, which are located on the exterior surface of AAMA. When the exterior surface of AAMA reaches saturation, Cd^{2+} gradually enters into the interior of AAMA. As the interspace becomes smaller, Cd^{2+} diffusion resistance becomes larger, resulting in the decrease of diffusion rates ($K_{id,2}$). The final stage corresponds to the equilibrium period, in which the adsorption and desorption rates are equal (Li et al. 2011).

Effect of initial concentration on the adsorption capacity

The effect of initial Cd^{2+} concentration on the adsorption capacity of AMAA is shown in Figure 12. As shown in Figure 12, the adsorption capacity for Cd^{2+} starts with a rapid increase and then increases slowly in the late stage. The maximum adsorption capacity of AMAA for Cd^{2+} has reached 167 mg/g at the initial concentration of 200 mg/L. AAMA can adsorb more Cd^{2+} in the ion cavities with increasing initial concentration. However, the adsorption capacity of AAMA for Cd^{2+} has a certain critical amount of ion cavities. The ion cavities are gradually filled with Cd^{2+} when the initial concentration increases to a certain value. As the initial concentration of Cd^{2+} increases further, the adsorption capacity remains at a relatively stable value. Compared with the adsorption capacity of metal ions by alginic acid, the adsorption capacity of Cd^{2+} by AAMA is
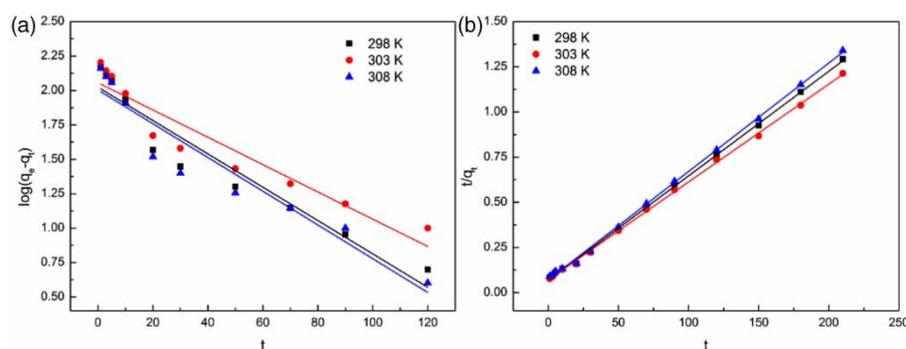

Figure 10 │ Pseudo-first-order kinetic model (a) and pseudo-second-order kinetic model (b) for the adsorption of Cd²⁺ onto AAMA.

Table 3 │ Dynamic parameters for the adsorption of Cd²⁺ onto AAMA at different temperature

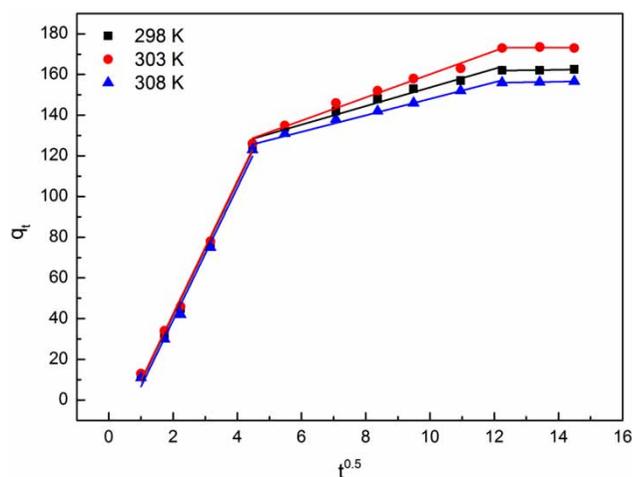| Temperature	Pseudo-first-order			Pseudo-second-order		
	K_1	q_e	R^2	K_2	q_e	R^2
298 K	0.0279	105.75	0.9082	4.99×10^{-4}	172.71	0.9992
303 K	0.0229	114.05	0.8816	4.13×10^{-4}	184.50	0.9991
308 K	0.0282	100.89	0.8973	5.13×10^{-4}	166.67	0.9989

Figure 11 | Intra-particle diffusion model for the adsorption of Cd²⁺ onto AAMA.

smaller (Vaid *et al.* 2015). This might be because the adsorption of Cd²⁺ by AAMA is dependent on ion holes and chemical adsorption, and ion holes are evenly distributed in the AAMA sphere. There is a certain steric hindrance for Cd²⁺ to enter AAMA, resulting in some ion holes not being used. So the adsorption capacity of AAMA is reduced compared to the adsorption capacity of alginic acid.

Adsorption isotherms

The adsorption isotherms are often used to explore the adsorption mechanism at different initial concentrations. The Langmuir, Freundlich, Dubinin-Raduskevich and Redlich-Petterson model are applied to describe the adsorption isotherm behavior.

The adsorption isotherms of Cd²⁺ with corresponding Freundlich, Langmuir Dubinin-Raduskevich and Redlich-Petterson plots are shown in Figure 12 and Figure S3. The fitting parameters of both Freundlich and Langmuir isotherms are shown in Table 5 and Table S2. From Table 5 and Table S2, it can be found that the correlation coefficients of Langmuir were highest among the Freundlich, Dubinin-Raduskevich, and Redlich-Petterson models. This indicated that the adsorption progress is monolayer and homogeneous

(Pang *et al.* 2011b). The forecast maximum adsorption capacity of AAMA by the Langmuir model for Cd²⁺ is 181.82 mg/g, which is higher than previously reported adsorbents (Table 6). In addition, the values of dimensionless constant R_L ranged from 0.12 to 0.34 for Cd²⁺, suggesting that the adsorption of Cd²⁺ is considered as favorable.

Adsorption thermodynamics

Thermodynamic parameters such as free energy change (ΔG^0), entropy change (ΔS^0) and enthalpy change (ΔH^0) can be calculated by Equations (2)–(4).

$$K_d = \frac{q_e}{C_e} \tag{2}$$

$$\ln K_d = \frac{\Delta S^0}{R} - \frac{\Delta H^0}{RT} \tag{3}$$

$$\Delta G^0 = \Delta H^0 - T \cdot \Delta S^0 \tag{4}$$

where C_e(mg/L) and q_e(mg/L) are the concentration and the adsorption capacity of AMAA under equilibrium condition.
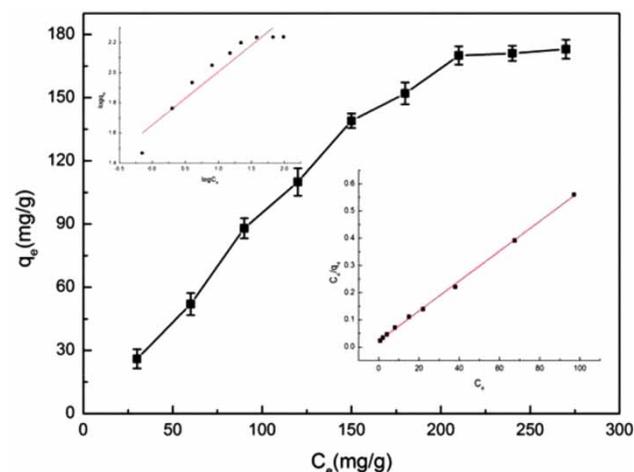

Figure 12 | Effect of initial concentration on the adsorption capacity (experimental conditions: pH = 5, contact time is 140 min, 100 mg AAMA in 100 mL solution at 303 K, repeat time: 3).

Table 4 | Intra-particle diffusion model parameters for the adsorption of Cd²⁺ onto AAMA

Temperature	First linear portion			Second linear portion		
	Kd_1	C_1	R_1^2	Kd_2	C_2	R_2^2
298 K	32.6754	−23.3412	0.9920	4.5665	107.9714	0.9693
303 K	32.6549	−22.8904	0.9929	5.6895	103.2264	0.9829
308 K	32.5933	−25.9351	0.9900	4.0529	107.5182	0.9709

Table 5 │ Isotherm modeling parameters for the adsorption of Cd^{2+} onto AAMA

Adsorbent	Langmuir isotherm model				Freundlich isotherm model		
	q(mg/g)	K_L	R_L	R^2	K_F	n	R^2
AAMA	181.82	0.2443	0.12–0.34	0.9990	45.03	2.84	0.8876

Table 6 │ Adsorption comparison of AAMA and reported studies on adsorbents for Cd^{2+}

| Adsorbent	pH	T(°C)	C_0 (mg/L)	Adsorption capacity (mg/g)	References
Modified silica particle	6	25	150	55.56	Radi et al. (2015)
l-arginine modified adsorbent	6	25	210	120.2	Guo et al. (2017)
Inverse emulsion polymerization:	7	30	250	107	Zhu et al. (2017)
AAMA	5	30	200	175	In this work

T (K) is the temperature. The fitted linear by $\ln K_d - 1/T$ is shown in Figure 13. Table 7 shows the related parameters for the adsorption process. As shown in Table 7, ΔG^0 has negative values. ΔH^0 and ΔS^0 have positive values in the range of 293–303 K, while ΔH^0 and ΔS^0 have negative values. The activation energy can be defined by the Arrhenius equation. The linear expression is:

$$\ln K_2 = -\frac{E_a}{RT} + \ln K_0 \tag{5}$$

where K_2 is the rate constant of the pseudo-second-order model, E_a is the activation energy of adsorption, T is temperature, and K_0 is the temperature influence factor. The linear fitted by $\ln K_2 - 1/T$ is shown in Figure 13. The activation energy of Cd^{2+} adsorbed on the surface of AAMA is 41.26 kJ/mol. This suggested that both chemisorption and physical adsorption are involved in the adsorption of Cd^{2+} by AAMA. Chemical adsorption is the main mechanism, while physical adsorption is the auxiliary (Cao et al. 2017).

Adsorption mechanism

The ion cavity is very important in the adsorption mechanism of adsorption of Cd^{2+} by AAMA. In order to confirm the role of functional groups in the adsorption mechanism, the XPS survey spectrum before and after adsorption (named AAMA and AAMA-Cd^{2+}) and high resolution XPS scans of N1 s, O1 s and C1 s were investigated.
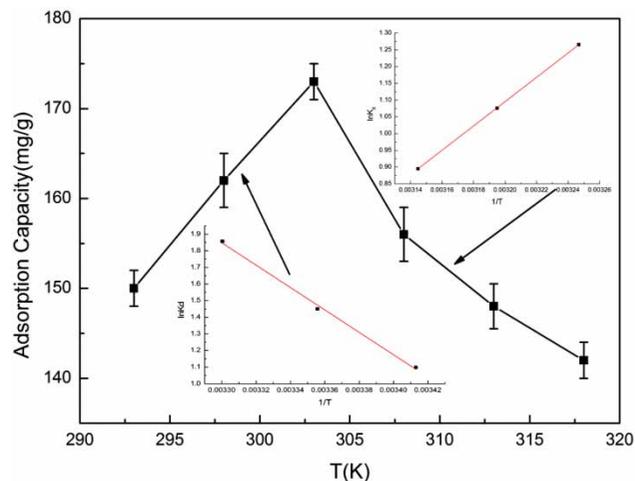
Figure 13 │ Effect of temperature on adsorption capacity (experimental conditions: metal ion concentration is 200 mg/L, pH = 5, contact time is 140 min, 100 mg AAMA in 100 mL solution, repeat time: 3).

Table 7 │ The related thermodynamic parameters for the adsorption of Cd^{2+} onto AAMA

T(K)	ΔG^0	ΔH^0	ΔS^0	R^2
293	−2.63	55.97	0.20	0.9945
298	−3.63			
303	−4.63			
308	−3.35	−30.15	−0.087	0.9999
313	−2.92			
318	−2.48			

The survey scans' XPS spectra of AAMA and AAMA-Cd^{2+} are shown in Figure 14(a). From Figure 14(a), it can be found that the elements of Fe, O, N and C were detected. After Cd^{2+} adsorption, a new intense peak for Cd at 400.5 eV was detected, suggesting Cd^{2+} was successfully adsorbed on AAMA. The high resolution O 1 s, N1 s and C1 s spectra of AAMA are shown in Figure 14(b), 14(d) and 14(f). For the AAMA before adsorption, there are two peaks for O1 s spectra, corresponding to 529.6 and 531.4 eV. The peak at 529.6 was related to amide (O = C–N). The peak at 531.4 eV can be attributed to carboxyl (COO⁻) (He et al. 2016). The contents of the above oxygen atoms before adsorption were 32.96% and 67.04%,
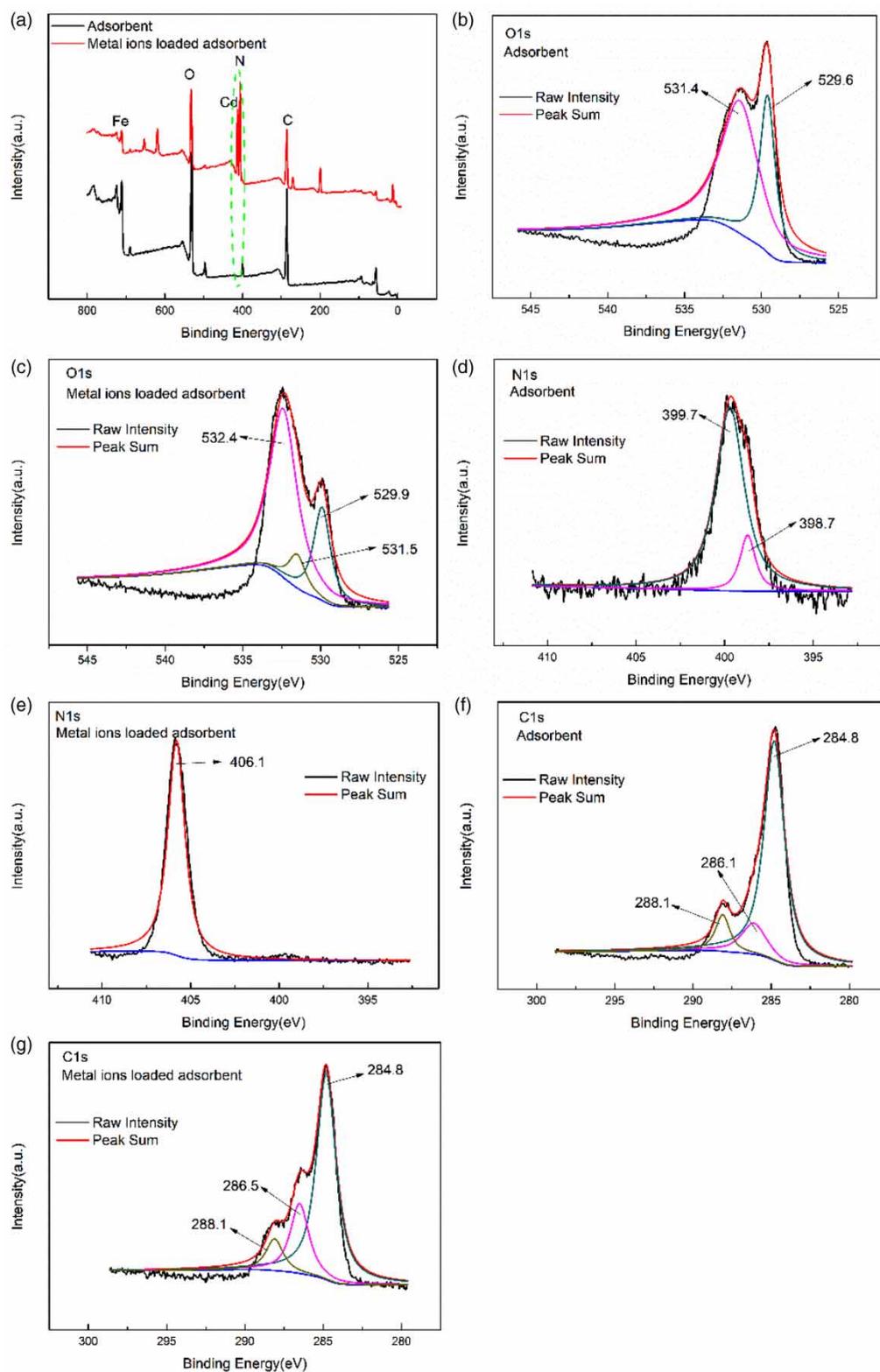
Figure 14 │ The survey scan XPS spectra (a) and high-resolution scan XPS spectra of O1s (b) N 1 s (d) C 1 s (f). O1 s (c), N 1 s (e) and C 1 s (g) of AAMA after adsorption of Cd^{2+}.

respectively. After Cd^{2+} adsorption, a new peak disappeared at 532.4 eV (Figure 14(c)). The contents of the three peaks turned to be 28.80% (529.6 eV), 8.49% (531.4 eV) and 62.71% (532.4 eV). This proved that the content of the oxygen atoms in the carboxyl group decreased after Cd^{2+} adsorption, while the content of carbonyl increased because of the formation of the Cd^{2+}–O–C $=$ O group. The C 1 s spectrum was constituted by three peaks, corresponding to a peak at 284.8 eV (C-C), a peak at 286.1 eV (amide (NH_2–C $=$ O)), and a peak at 288.1 eV (carbonyl (C $=$ O)). The contents of the above carbon atoms before adsorption were 9.12%, 13.34%, and 77.54%, respectively, while their contents became 9.19%, 21.83%, and 68.98% after Cd^{2+} adsorption (Figure 14(e)). This suggested that the carbonyl group participated in the coordination reaction. The N1 s spectrum was composed of two peaks, corresponding to a peak at 399.7 eV (N-H) and a peak at 398.7 eV (C-N). The contents of the above nitrogen atoms before adsorption were 85.76% and 14.23%, respectively, while their contents became 100% (406.1 eV) after heavy metal ion adsorption (Figure 14(g)). This indicated that the amino was reacted with Cd^{2+}. The O1 s, N1 s and C1 s peak areas of AAMA before and after Cd^{2+} adsorption were different. These results suggested that carboxyl and amino play a vital role in the Cd^{2+} adsorption progress. In other words, AAMA selectively adsorbs Cd^{2+}, which not only relies on ion holes, but also depends on functional groups.

Desorption and regeneration

The recyclability of the adsorbent is a very important parameter for evaluating the potential for industrial applications. The regeneration and reuse of AAMA for Cd^{2+} removal was evaluated. Because of the strong chelating ligand between EDTA and metal ions, it was used as the desorption solvent in this study. AAMA can be regenerated by 0.5 M EDTA. The adsorption capacity of five cycles was 175, 163, 145, 131 and 125 mg/g, respectively. and still keep about 71% adsorption capacity in the fifth cycle of regeneration (Figure 15). The slight decrease in adsorption capacity may be due to two reasons. Firstly, active sites of chemical adsorption are lost in the process of repeated use. Secondly, the specific geometry structure of AAMA and ion holes is destroyed in the process of repeated use, resulting in a decrease in the number of ion holes and a change in the spatial size of ion holes, which makes it difficult to accurately and selectively adsorb Cd^{2+}. Other adsorbents have also found that the adsorption capacity decreases slightly with increasing recycle time. The adsorption capacity of AMAA

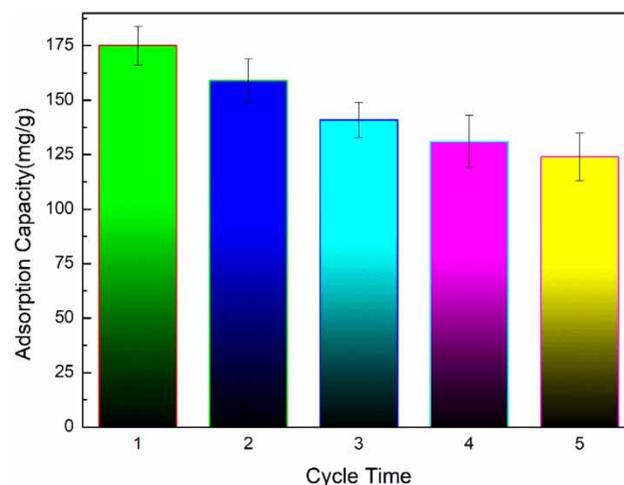**Figure 15** | Cycle adsorption experiments of Cd^{2+} by AAMA (experimental conditions: metal ion concentration is 200 mg/L, contact time 140 min, pH $=$ 5, 100 mg AAMA in 100 mL solution at 303 K, repeat time: 3).

for Cd^{2+} removal changed slightly, which might be due to the loss of active sites and the specific geometry structure being damaged in the adsorption/desorption/regeneration processes (Jing *et al.* 2015). These results suggested that AAMA has a good potential for industrial applications.

CONCLUSION

According to the data exposed above, the following conclusions can be drawn:

(1) SEM, TEM, TGA, XRD, and VSM were employed to characterize AAMA. This proved that Cd^{2+} imprinted alginic acid and polymers magnetic adsorbent has been successfully prepared.

(2) The adsorption capacity of AAMA was investigated by the different factors. These results revealed that AAMA had optimum adsorption capacity at a temperature of 303 K, initial concentration of 200 mf/L, and pH of 5.0. The adsorption capacity of AAMA for Cd^{2+} was more than 4.79 times that for other metal ions, suggesting its selectivity for the adsorption of Cd^{2+}.

(3) The experimental data were well described by the pseudo-second-order kinetic model and Langmuir isotherm model. The maximum adsorption capacity for Cd^{2+} can reach 175 mg/g. The parameters of adsorption thermodynamics concluded that the adsorption progress is endothermic and spontaneous in nature.

(4) The parameters of adsorption activation energy suggested that there is chemisorption and physical adsorption involved in the adsorption of AAMA

selectively adsorbs Cd^{2+}, which not only relies on ion holes, but also depends on functional groups.

DATA AVAILABILITY STATEMENT

All relevant data are included in the paper or its Supplementary Information.

REFERENCES

Ahmaruzzaman, M. 2011 Industrial wastes as low-cost potential adsorbents for the treatment of wastewater laden with heavy metals. *Adv Colloid Interface Sci* **116**, 36–59.

Cao, C. Y., Liang, C. H. & Yin, Y. 2017 Thermal activation of serpentine for adsorption of cadmium. *J Hazard Mater* **329**, 222–229.

Fan, S., Zhou, J., Zhang, Y., Feng, H., Hu, H., Huang, Z. & Qin, Y. 2020 Preparation of sugarcane bagasse succinate/alginate porous gel beads via a self-assembly strategy: improving the structural stability and adsorption efficiency for heavy metal ions. *Bioresource Technology* **306**, 123128.

Ge, H. C. & Huang, S. Y. 2010 Microwave preparation and adsorption properties of EDTA-modified cross-linked chitosan. *J Appl Polym Sci* **115**, 514–519.

Ge, H. C., Chen, H. & Huang, S. Y. 2012 Microwave preparation and properties of O-crosslinked maleic acyl chitosan adsorbent for Pb^{2+} and Cu^{2+}. *J Appl Polym Sci* **125**, 2716–2723.

Ge, H. C., Hu, T. T. & Chen, X. D. 2016 Selective adsorption of lead on grafted and crosslinked chitosan nanoparticles prepared by using Pb^{2+} as template. *J Hazard Mater* **308**, 225–232.

Guo, S. Z., Jiao, P. P. & Dan, Z. G. 2017 Preparation of *L*-arginine modified magnetic adsorbent by one-step method for removal of Zn(II) and Cd(II) from aqueous solution. *Chem Eng J* **317**, 999–1011.

Guo, S. Z., Zhang, F., Li, D. & Jiao, P. P. 2020 Highly efficient and selective removal of cadmium from aqueous solutions based on magnetic graphitic carbon nitride materials with molecularly imprinted polymers. *J Mol Struct* **1221**, 128887.

He, J., Cai, X. & Chen, K. 2016 Performance of a novelly-defined zirconium metal-organic frameworks adsorption membrane in fluoride removal. *J Colloid Interface Sci* **484**, 162–172.

Jing, Y. J., Yin, N. N. & Yu, X. Q. 2015 Pb(II)-imprinted chitosan beads to enhance the adsorption property and selectivity: characterization, kinetics, and thermodynamics. *Desalin Water Treat* **56**, 1–10.

Lee, S. M., Laldawngliana, C. & Tiwari, D. 2012 Iron oxide nano-particles immobilized sand material in the treatment of Cu(II), Cd(II) and Pb(II) contaminated waste waters. *Chem Eng J* **195**, 103–111.

Lenoble, V., Meouche, W. & Laatikainen, K. 2015 Assessment and modelling of Ni(II) retention by an ion-imprinted polymer: application in natural samples. *J Colloid Interface Sci* **448**, 473–481.

Li, G., Zhao, Z. & Liu, J. 2011 Effective heavy metal removal from aqueous systems by thiol functionalized magnetic mesoporous silica. *J Hazard Mater* **1**, 277–283.

Ma, Z. Y., Guan, Y. P. & Liu, H. Z. 2005 Synthesis and characterization of micron-sized monodisperse superparamagnetic polymer particles with amino groups. *J Polym Sci Part A: Polym Chem* **43**, 3433–3439.

Mahesh, U., Chhatbar, R. M. & Kamalesh, P. 2011 Microwave-induced facile synthesis of water-soluble fluorogenic alginic acid derivatives. *Carbohyd Res* **346**, 527–533.

Mahmood, T., Saddique, M. & Naeem, A. A. 2011 Comparison of different methods for the point of zero charge determination of NiO. *Ind Eng Chem Res* **50**, 10017–10023.

Mishra, S. & Verma, N. 2017 Surface ion imprinting-mediated carbon nanofiber-grafted highly porous polymeric beads: synthesis and application towards selective removal of aqueous Pb(II). *Chem Eng J* **313**, 1142–1151.

Mittal, H., Maity, A. & Ray, S. S. 2015 Synthesis of co-polymer-grafted gum karaya and silica hybrid organic–inorganic hydrogel nanocomposite for the highly effective removal of methylene blue. *Chem Eng J* **279**, 166–179.

Pandi, K. & Viswanathan, N. 2015 A novel metal coordination enabled in carboxylated alginic acid for effective fluoride removal. *Carbohydr Polym* **118**, 242–249.

Pang, Y., Zeng, G. & Tang, L. 2011a Preparation and application of stability enhanced magnetic nanoparticles for rapid removal of Cr(VI). *Chem Eng J* **175**, 222–227.

Pang, Y., Zeng, G. & Tang, L. 2011b PEI grafted magnetic porous powder for highly effective adsorption of heavy metal ions. *Desalination* **281**, 278–284.

Pawar, S. N. & Edgar, K. J. 2012 Alginate derivatization: a review of chemistry, properties and applications. *Biomaterials* **33** (11), 3279–3305.

Radi, S., Tighadouini, S. & Massaoudi, M. E. 2015 Thermodynamics and kinetics of heavy metals adsorption on silica particles chemically modified by conjugated-ketoenolfuran. *J Chem Eng Data* **60**, 2915–2925.

Rahmi, L. & Nurfatimah, R. 2018 Preparation of polyethylene glycol diglycidyl ether (PEDGE) crosslinked chitosan/activated carbon composite film for Cd^{2+} removal. *Carbohydr Polym* **199**, 499–505.

Uddin, M. K. 2017 A review on the adsorption of heavy metals by clay minerals, with special focus on the past decade. *Chem Eng J* **308**, 438–462.

Vaid, U., Mittal, S. & Nagendra, B. J. 2015 Influence of anion induced protonabstraction on Cu(II) adsorption by alginic acid. *React Funct Polym* **97**, 48–55.

Yong, S. K., Bolan, N. & Lombi, E. 2013 Synthesis and characterization of thiolated chitosan beads for removal of Cu(II) and Cd(II) from wastewater. *Water Air Soil Pollut* **224**, 1–12.

Zhu, F., Li, L. W. & Xing, J. D. 2017 Selective adsorption behavior of Cd(II) ion imprinted polymers synthesized by microwave-assisted inverse emulsion polymerization: adsorption performance and mechanism. *J Hazard Mater* **321**, 103–110.